Unraveling the Resistive Switching Mechanisms in LaMnO3+δ-Based Memristive Devices by Operando Hard X-ray Photoemission Measurements

Benjamin Meunier, Eugénie Martinez, Raquel Rodriguez-Lamas, Dolors Pla, Monica Burriel, Carmen Jimenez, Yoshiyuki Yamashita, Olivier Renault

Unraveling the resistive switching mechanisms in LaMnO$_{3+\delta}$-based memristive devices by *operando* hard X-ray photoemission measurements

Benjamin Meunier[1]*, Eugénie Martinez[2], Raquel Rodriguez-Lamas[1], Dolors Pla[1], Monica Burriel[1], Carmen Jimenez[1], Yoshiyuki Yamashita[3], Shigenori Ueda[3], Olivier Renault[2]

[1]University Grenoble Alpes, CNRS, LMGP, F-38000 Grenoble, France

[2] University Grenoble Alpes, CEA, Leti, F-38000 Grenoble, France

[3]National Institute for Materials Science, Tsukuba, Ibaraki 305-0044, Japan

Abstract

Manganite-based devices have shown promising resistive switching properties, which performance strongly depends on the electrodes used to build them. Their nature affects the physical properties of the metal/manganite interfaces, leading to a different resistive switching responses and mechanisms, which are difficult to fully understand using conventional *ex situ* characterization techniques. Here, the switching mechanisms taking place in LaMnO$_{3+\delta}$-based memristive devices with a noble metal top electrode have been studied using an *operando* high energy x-ray photoelectron spectroscopy (HAXPES). The difference between HAXPES spectra obtained for devices in different resistance states, has allowed to elucidate the redox mechanism taking place in the devices. The HAXPES spectra indicate a reduction (oxidation) of the interfacial LMO when switching from high to low (from low to high) resistance states. The presence of an inert electrode instead of an oxidizable one, results in oxygen being released out of the lattice, instead of reacting with the electrode. Complementary, HAXPES energy shifts induced by the electric field has been used to probe the resistance drop inside the device at different position and for different resistance state.

1. Introduction

Hard x-ray photoelectron spectroscopy (HAXPES) is a powerful tool for *operando* non-destructive interface characterization of functional devices. The use of hard X-ray synchrotron radiation (2.4-12 keV) allows to gather information from regions up to 5 times deeper in the sample than with laboratory sources (e.g., Al-Kα), which is of particular interest to study the buried, often critical interfaces of a device covered by a thick electrode. *Operando* measurements, consisting in biasing a functional device (capacitor, memory cell, etc) while performing HAXPES, are, therefore, powerful in order to understand the changes in elemental composition and charge distribution inside the device during operation. Additionally, it confers to HAXPES analysis the necessary reliability for its application to device technology. This approach was already implemented for studying the interface polarization in a piezoelectric Pt/Ru/PbZr$_{0.52}$Ti$_{0.48}$O$_3$ high-density capacitor.[1] Oxide-based memristive devices could also take advantage of the excellent capabilities of *operando* HAXPES as the resistive switching mechanism occurring in such devices is often triggered by surface/interface processes. HAXPES has been employed to study the buried interfaces of different oxide-based memristive devices such as TiN/Hf$_{0.5}$Zr$_{0.5}$O$_2$,[2] Pt/Ti/Pr$_{0.5}$Ca$_{0.5}$MnO$_3$,[3] Au/Fe:SrTiO$_3$/Nb:SrTiO$_3$,[4] TiN/Pt/NiO.[5] and Ti/HfO$_x$.[6,7] Only the later work, however, has been subject to measurements in *operando* mode with *in situ* electrical characterization, while the others studied these interfaces after cycling operation.[8]

Among the plethora of oxides enabling resistive switching (RS), the switching response of the non-stoichiometric transition metal oxide LaMnO$_{3+\delta}$ (LMO) has been reported to be governed by the oxygen vacancies concentration in the material.[9,10] The apparent oxygen excess in LMO is ascribed to the formation of La and/or Mn cation vacancy sites (i.e., La$_{1-x}\square_x$,Mn$_{1-y}\square_y$O$_3$,

viz. LaMnO$_{3+\delta}$), where □ represents cation vacancies, and charge neutrality remains fulfilled thanks to the coexistence of Mn^{3+}/Mn^{4+} oxidation states.[11,12,13,14] Therefore, the valence state of the material is strongly correlated to the oxygen content, and Mn^{4+} can be seen as an intrinsic dopant.[15]

We recently investigated the microscopic mechanisms of local interfacial RS in LaMnO$_{3+\delta}$ by conductive atomic force microscopy (c-AFM)[16] and demonstrated that the change in resistance is associated with a drift of oxygen ions to the surface and the concomitant variation in the Mn valence state, resulting in modifications in the transport mechanism. However, the experimental configuration used in this work presents several specificities (e.g., low current density, bare surface, large active area, etc) that do not match the requirements of a standard functional device. For this reason, we then performed a first set of *operando* HAXPES measurements on a TiN/LMO/Pt prototypical memory cell.[17] In this work, we monitored the redox reactions occurring at the TiN/LMO interface during RS. In this case, the TiN top electrode acts as a reservoir in which oxygen is stored when LMO is in high resistance state (HRS) and released during the switch back to low resistance state (LRS). From the HAXPES and electrical characterization we deduced that the switching mechanism was localized at the TiN/LMO interface. However other relevant electrode, but noble (e.g. Au, Pt, Pd) or semi-noble (Cu) metals, are also commonly used for building memory, and also display RS behavior. Since such materials have a low oxygen affinity, the question arises on how the resistive switching mechanism is affected by the absence of an oxygen reservoir interlayer.

In the present contribution we report the recent work on M/LMO/Pt stack with M = Au or Pd by means of *operando* HAXPES. We focus here on the behavior of a memory cell with a chemically inert electrode, compared to the previously reported LMO covered by an oxidizable TiN electrode. We propose a model explaining how an oxygen reservoir at the interface with the electrode is created during RS in the presence of a noble metal as top electrode. The results clearly illustrate that the electrode material has an impact on the nature of the oxygen reservoir necessary for multiple RS operation and thus on the associated switching mechanism itself.
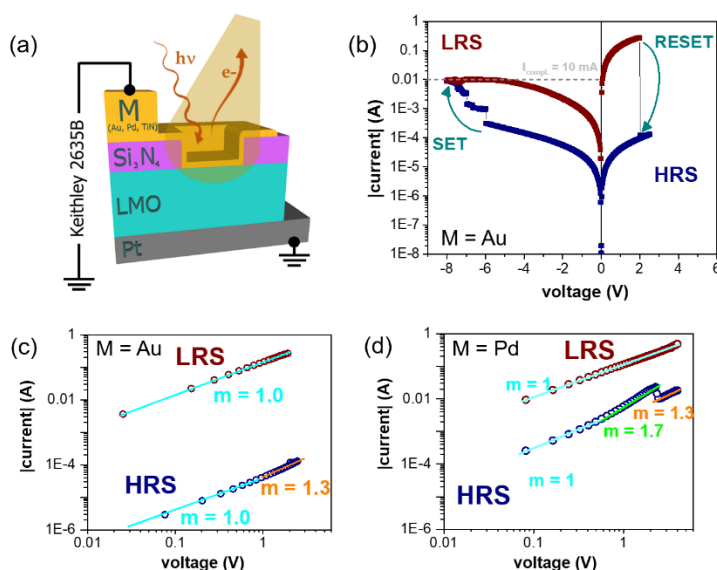
Experimental

Figure 1 *(a) sketch of the operando memristive device where the Pt bottom electrode is grounded and the metal top electrode is biased. (b) In situ I−V characteristics obtained for an Au/LMO/Pt stack with a current compliance of 10 mA. (c) and (d) log(I)-log(V) plots*

The LMO thin film (100 nm-thick) used for this study was grown by pulsed injection metal-organic chemical vapor deposition following the strategy III of Ref.[18] The structural characterization of the LMO thin film is presented in **Figure S1** of **Supporting Information**. In order to both match the HAXPES requirements and allow *in situ* electrical characterization, the device depicted in **Figure 1(a)** was fabricated. The active region consists of a thin (~7 nm) metal layer (Au or Pd) deposited directly on a 100x100 µm² LMO surface. Outside this region, the top electrode was electrically isolated from LMO by a 50 nm thick, sputtering-deposited Si_3N_4 insulating layer. 300 µm away from this active area, a thick current collector of the same material as the electrode was deposited, wire-bonded to the sample-holder, and eventually connected to a sourcemeter (Keithley 2635B). The Pt bottom electrode was also wire-bonded to the grounded contact pad of the sample-holder. Once in the HAXPES chamber, an additional small series resistance was measured due to the long distance between the chamber and the end station control cabin. By comparing the resistance measured directly at the sample's output and for a sample mounted on the sample holder in the analysis chamber, the total external resistance was measured to be R_{ext} = 2.5 Ω.

HAXPES measurements were performed at the BL15XU beamline of the SPring-8 synchrotron facility (Hyogo, Japan). The photon energy was set to 7933.5 eV (as determined from the Fermi level of the Au top electrode of one of the device) The X-rays were monochromatized by a Si(111) double crystal and post monochromator (channel cut crystal). The beam cross-section was estimated to 100×30 µm², with take-off angle of 70°, the effective footprint of the beam on the sample surface was 400x30 µm². The photoelectrons were detected by a high-resolution hemispherical analyzer (VG Scienta R4000) providing an overall energy resolution of 240 meV as measured by the Fermi cutoff of an Au film which also defined the binding energy (BE) scale. The projected beam could be selectively directed onto either a single memory device or the bare LMO film.

2. Results and discussion

2.1. Resistive switching of the M/LMO/Pt devices (M=Au,Pd)

Once the sample described in Figure 1a was mounted and introduced into the analysis chamber under Ultra High Vacuum (UHV) condition (~10^{-7} Pa), electrical measurements were performed. **Figure 1b** shows the characteristic hysteretic current-voltage (*I-V*) curve measured *in-situ* by cyclic voltammetry for Au top electrode-memristive device. The device exhibits an asymmetric bipolar counter-clockwise-type switching without requiring an electroforming step. Noticeable differences are observed between the SET and RESET processes. An abrupt RESET from LRS (R_{LRS} = 7.2 Ω) to HRS (R_{HRS} = 22 kΩ) occurs for positive polarity at ~2.0 V for a corresponding high to low resistance ratio of four orders of magnitude. Conversely, the SET process requires higher voltage in negative polarity and, instead of a single abrupt switch, it presents several consecutives steps starting at ~ -6 V. The compliance current was set to 10 mA in negative polarity in order to avoid the oxide electrical breakdown at high voltage (1A expected at -10V for R = R_{LRS}). With this limitation, a decrease of the resistance of only two orders of magnitude is observed after the SET process. However, similar measurements performed *ex situ* (**Figure S2**) on other devices reveal that the resistance can be decreased to its initial value by increasing the current limit and that, in these conditions, several SET-RESET cycles can be obtained.

The log-log representation of the *I-V* curve in Figure 1c shows two linear regimes associated with two slopes: m = 1 and m > 1. The m = 1 case corresponds to ohmic transport in the device. It is observed in the initial LRS branch and at low voltage in HRS ($|V_{appl.}|$ < 1 V). The presence of a non-ohmic behavior after RESET indicates a modification of the transport mechanism due to the switching process, as discussed in our previous works.[16,17]

In situ electrical measurements have been performed the same way on the memristive device with a Pd top electrode. The corresponding log-log I-V curve depicted in Figure 1d shares similar features with the Au top electrode one, i.e. an ohmic behavior in the LRS and at low voltages in the HRS. The most noticeable difference between the two metal electrodes is the high to low resistance ratio of "only" two orders of magnitude for Pd with R_{LRS} = 8.6 Ω and R_{HRS} = 225 Ω, compared to the 4 orders of magnitude observed for Au, although the associated conduction mechanism is assumed to be the same irrespective of the electrode material. These observations are also supported by the I-V curves obtained on LMO samples from similar *ex situ* measurements in standard metal/LMO/Pt devices with square top electrodes (see FigureS2 of Supporting Information). The similarity in the I-V characteristics demonstrates that the samples are not affected by the *operando* conditions (UHV and high energy radiation), at least as far as the first resistive switching operations are concerned. Having an ohmic behavior in low voltage range for both electrode in HRS and LRS indicates that the transport and switching mechanisms are different from the one reported when using TiN electrode in which case RS was driven the change of the electrode/interface state and resistance.[17] Moreover, the devices with inert metal electrodes (Au or Pd) present a larger resistive switching amplitude (of several orders of magnitude) compared to the one observed in our previous study using TiN (R_{HRS}/R_{LRS}=4).

2.2. HAXPES study of M/LMO/Pt devices in the virgin state

Prior to the *operando* measurements, the LMO bare surface was analyzed. **Figure 2** presents the O 1s, La $3d_{5/2}$ and Mn 3s core levels. A Shirley-type background was subtracted from all the spectra. Peak fitting was performed using pseudo-Voigt functions.

The O 1s spectrum in Figure 2a. consists of two contributions, $O_{latt.}$ (529.4 eV) and $O_{inter.}$ (531.8 eV) corresponding to lattice oxygen from the LMO and interfacial oxygen (oxygen outside of the lattice, for instance adsorbed oxygen on a bare surface), respectively. This model for O 1s deconvolution in LMO has been widely used by electrochemists to study the $LaMnO_3$ as oxygen catalyst.[19,20] The remarkable catalytic activity and stability of LMO is directly related to the noticeable and stable presence of adsorbed oxygen on its surface.[21]

The La 3d photoelectron peak of lanthanum compounds shows very prominent satellite features due to core−hole screening processes triggered by charge transfer between the unoccupied 4f valence orbitals and 2p orbitals of oxygen.[22,23] Thus, in the resulting La$3d_{5/2}$ spectrum, a main peak (cf^0) and two satellite peaks (cf^1L) show up, where c and L denote a core-hole in the La $3d_{5/2}$ states and a ligand O 2p hole, respectively.[24] In our previous study, we demonstrated the direct relationship between the oxygen content in the La surrounding and the ratio of the satellites/main peak areas.[16]

The Mn 3s core levels are split into two contributions due to differences in the 3s-3d electrostatic exchange interaction between spin-up ($3s^\uparrow$) and spin-down ($3s^\downarrow$) states after photoemission.
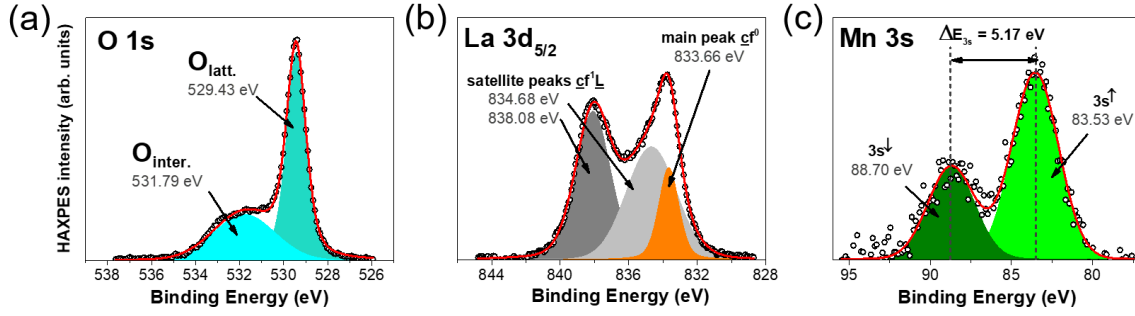
Figure 2 *HAXPES spectra of O1s (a), La 3d5/2 (b) and Mn 3s (c) core levels of a pristine LMO surface.*

The energy separation between the $3s^\uparrow$ and the $3s^\downarrow$ component in the 3s core level spectrum may be expressed by the Van Vleck's theorem as:[25]

$$\Delta E_{Mn3s} = (n+1)G^2(3s3d) \tag{1}$$

Where *n* is the number of unpaired 3d electrons and G^2 the Slater exchange integral.

The energy separation increases linearly against *n* as long as the nature of the ligands is the same.[26] Data reported in the literature give an average multiplet splitting of 5.4 eV for pure Mn^{3+} states and 4.4 eV for pure Mn^{4+} states.[27,28] Thus, in our case, the estimated valence of manganese is 3.2 ±0.05 for a measured peak separation of ΔE_{Mn3s} = 5.17 eV.

According to the device description of Figure 1, after fabrication the LMO surface was locally covered by a thin metal layer, either Au or Pd depending on the device. In this configuration, electrical measurements and HAXPES analyses can be performed simultaneously in so-called *operando* conditions. **Figure 3** presents the Au $4f_{7/2}$ and $Pd_{5/2}$ 3d HAXPES spectra of the corresponding memristive devices for different applied voltages ($V_{appl.}$ = 0, ±1V).
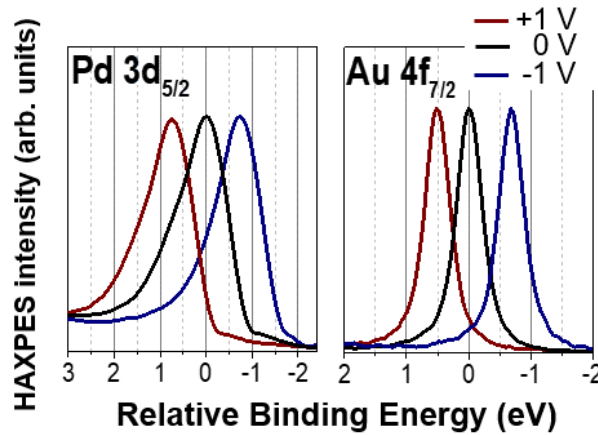

Figure 3 *HAXPES shift of Pd 3d$_{5/2}$ and Au 4f$_{7/2}$ for the M/LaMnO$_{3+\delta}$ stacks (M=Au, Pd) for applied voltages of 0V and +/- 1V.*

The series of spectra provides evidence that the *operando* measurements are performed in reliable conditions. When a bias is applied, the photoelectrons kinetic energy is modified by the electrostatic potential and the measured energy levels are shifted accordingly. However, the shifts observed on the HAXPES spectra are smaller than the applied biases, due to the external series resistance resulting in a small bias drop across the circuit. The effective potential observed on the samples (V) for V_{appl} = +/-1V is equal to +/-0.7eV. The energy shift of a specific core level may be interpreted as the electrical potential "seen" at the location of the corresponding element in the device. As the metal electrode, Pd or Au, is located on top

of the whole device (see Figure 1a), the observed shift of each spectrum is directly related to the total resistance of the sample. Thus, for an applied voltage V_{appl} and a HAXPES energy shift V (= electrical potential), the equivalent resistance is calculated with the following potential divider relationship:

$$R = R_{ext} \cdot V/(V_{appl} - V) \tag{2}$$

with the external resistance R_{ext} = 2.5 Ω corresponding to the external resistance of the overall setup (wires, contacts, etc).

Considering the Pd 3d spectrum, the amplitude of the energy shift is the same for positive and negative polarities and is determined as 0.72 eV in the virgin state. The corresponding resistance for the whole Pd/LMO stack is R_{Pd+LMO} = 6.4 Ω. The energy shift for V_{appl} = +1 V gives a value of the LMO resistance with Au electrode of R_{Au+LMO} = 6.1 Ω, thereby similar to R_{Pd+LMO} with Pd electrode. The total resistance R_{LMO}+R_{ext} = 8.6 Ω is also in good agreement with the one electrically measured in LRS.

2.3. Operando measurements of the Pd/LMO/Pt stack

From the HAXPES measurements under applied electric field it was observed that not only the spectra of the metal electrode shift due to the applied electric field, but also those characteristics of the LMO film itself. For the LMO elements, unlike for Au or Pd, the peak shifts also include chemical state- and/or composition changes due to resistive switching triggered by the electric field.

For *operando* HAXPES measurements, we address only the results from the Pd/LMO/Pt device, as in the case of the Au top electrode, both La 3d and Mn 3s spectra overlap Au peaks, thereby hampering data interpretation (the La 3d core level is partially hidden by the asymmetric tail of the Au 4s signal and the Mn 3s peak overlaps the Au 4f line).
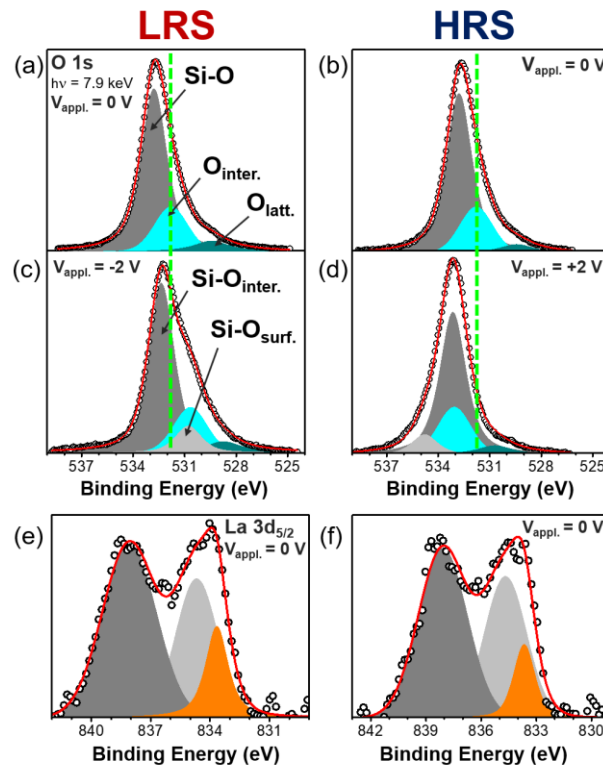

Figure 4 *O 1s spectra for the Pd/LMO/Pt stack in (a) LRS, and (b) HRS for different applied voltage (c) $V_{appl.}$ = -2 V and (d) $V_{appl.}$ = +2 V. La3d$_{5/2}$ spectra for the Pd/LMO/Pt stack in (e) LRS, and (f) HRS*

HAXPES measurements were carried out on a Pd/LMO/Pt device before and after switching. The La3d$_{5/2}$ and O1s core levels were measured, while the Mn 3s core-level was not recorded due to an overlapping with the Pd 3d one.

One of the goals of the *operando* measurements is to track small energy shifts in the photoemission spectra in complement with the chemical environment analysis. Therefore, it requires a proper and rigorous data treatment process. The following assumptions were made and applied as initial constraints during the O 1s fitting process:

- Peak fitting was performed using a combination of pseudo-Voigt functions with the Lorentzian to Gaussian ratio and the peak width kept constant for all the data sets.
- In open circuit conditions (V$_{appl}$=0 V), the O 1s spectra are fitted using the binding energies from the reference bare surface (see Figure2).
- For *operando* data (i.e. V$_{appl.}$ = +/-2 V) only the energy is a free parameter. Indeed, for the Pd electrode, the operating voltage is well under V$_{SET}$ or V$_{RESET}$ and no chemical change is expected.

The resulting fits are presented in **Figure 4** and the main parameters summarized in **Table 1**.

The O 1s spectra are dominated by the silicon oxide signal from the partially oxidized Si$_3$N$_4$ layer. Indeed, at the center of the 100x100 μm² Au electrode, the beam footprint is 400x30 μm^2 but the effective footprint is much larger due to the beam tail and X-ray diffusion through the surface material, explaining the presence of a Si-O component in the O 1s spectrum. When the device is biased, the Si-O contribution is split into two separate peaks (see Figure 4c-d). Oxidation of the Si$_3$N$_4$ surface occurs prior to electrode deposition. After device fabrication part of the native oxide is covered by the metal while the majority remains uncovered. Hence when a bias is applied on the top electrode, the covered part sees a larger electrical potential resulting in the shifted Si-O contribution Si-O$_{/Pd}$ in O 1s spectra, while the uncovered surface's contribution will not be shifted, and thus explaining the presence of these two contributions.

The two additional contributions to the O 1s spectrum (light blue and dark green contributions in Figure 4a-d) are specific to the LMO in the memristive device, and match well the O$_{latt.}$ and O$_{inter.}$ contributions from the bare surface (see Figure 2).

O 1s	Content (%)			Energy shift (eV)			
	Si-O	O$_{latt.}$	O$_{inter.}$	Si-O$_{/Pd}$	O$_{latt.}$	O$_{inter.}$	Si-O
Pristine	-			-	529.43	531.79	
LRS 0 V	71.8	7.7	20.5	-	-	-	
LRS -2 V	-	-	-	-2	-0.69	-1.13	-0.42
HRS 0V	71.8	6.6	21.6	-	-	-	
HRS +2 V	-	-	-	+2	+1.27	+1.27	+0.36

Table 1. *Relative content of each contribution in the O1s spectra (see Figure 4) and their energy shift when a ±2 V voltage is applied. Pristine refers to the bare surface presented in Figure 2.*

By comparing the O1s spectra measured in LRS and HRS in Figure 4a and 4b, respectively, noticeable differences are observed, though unfortunately partly screened by the large Si-O signal. For more details, Table 1 shows the relative area of each contribution. From LRS to HRS, the O$_{inter.}$ contribution slightly increases with respect to the O$_{latt.}$ one. We previously reported such a modification of the surface composition after RESET (LRS to HRS) operation performed on a bare LMO surface using a conductive AFM tip.[16] We concluded by the application of a positive bias (V$_{RESET}$ > 0) oxygen ions drift from the lattice towards the top electrode and remain adsorbed, triggering the change in resistance. At this point one may wonder what is the physical meaning of O$_{inter.}$ when the surface is covered by an electrode.

Some hints may be found in previous studies of oxide-based resistive switches revealing the formation of oxygen in gas form during switching operation. For instance, the growth of microscopic gas bubbles have been observed in $Pt/TiO_2/Pt$ during operation.[19] the formation of an oxygen pocket has even led to the deformation of the top electrode in a $Pt/SrTiO_3$ system.[29] In both cases, the electrode was made of a noble metal. However, to the best of our knowledge, such oxygen pockets/bubbles have never been reported using an inert electrode. Therefore, the O_{inter} contribution is ascribed to adsorbed at the metal/oxide interface, which could eventually lead to the formation of oxygen pockets. Thus, the increase of the $O_{inter.}$ contribution indicates that oxygen is released from the LMO lattice during RESET stage (V_{RESET} > 0). Complementing the literature example, observations of the surface of Au/LMO/Pt devices after several *ex situ* I-V cycles show that a lift-off of the electrode had occurred (see Supporting Information in **Figure S3** and **S4**). This deformation and eventual destruction of the top electrode could originate from the expansion of this gas pocket during the electrical measurements. This gas expansion may also be enhanced by Joule heating, keeping in mind that the LRS in LMO involves a large current density.

Figure 4c and 4d present the O 1s measured while applying a negative and positive voltage, respectively. The behavior of the Si-O signal has been previously explained, the shifts measured for the oxidized Si_3N_4 in contact with the electrode (Si-O/Pd) follows the one observed for Pd 3d. The energy shift of each contribution reported in Table 1 is in good agreement with our model: the deeper the contribution in the device, the lower the corresponding shift. The energy shifts in LRS show that $O_{inter.}$ and $O_{latt.}$ are not at the same electrical potential, indicating a noticeable potential drop between the top electrode and the LMO surface, and thus the presence of a LMO interfacial layer. In HRS the energy shifts of $O_{inter.}$ and $O_{latt.}$ are the same, but it cannot be concluded that the interfacial resistance vanishes since it may be screened by the large LMO resistance (as expected from Eq.2).

To complement these observations, Figure 4e and 4f show the La3d spectra recorded in LRS and HRS, respectively. By comparing them with the La 3d spectra from the bare surface it is observed that the main peak at 833.7 eV (orange peak) is less intense compared to its two satellites (in grey). This observation can be explained by an increase of the oxygen content. At the excitation energy of 7.93 keV, the estimated probing thickness (3xIMFP) by La 3d photoelectrons is 18 nm. Due to the presence of the 7 nm-thick top electrode in the device, the probing area into the LMO (about 10 nm) is less deep than when measuring a bare surface. Thus, the difference in the La 3d spectra indicates that the interface with Pd is more oxidized than the bulk LMO, in agreement with a more oxidized LMO surface commonly observed in this material.[30] This relative intensity between the main photoemission line and its two satellites is also the key parameter regarding the spectra modification between the LRS and HRS. A slight decrease of the main peak intensity is observed in HRS (Figure 4f), indicating an increase of the oxygen content in the La neighborhood. From the O 1s analysis it was previously deduced that oxygen ions drift to the top electrode/LMO interface under the effect of the electric field, and part of the oxygen is released from the LMO lattice as gas traps at the interface. The La spectra indicates that, in addition to the oxygen release, an oxygen-rich region is formed at the top LMO interface. Therefore, a good consistency is found among the whole set of photoemission results as interpreted here.
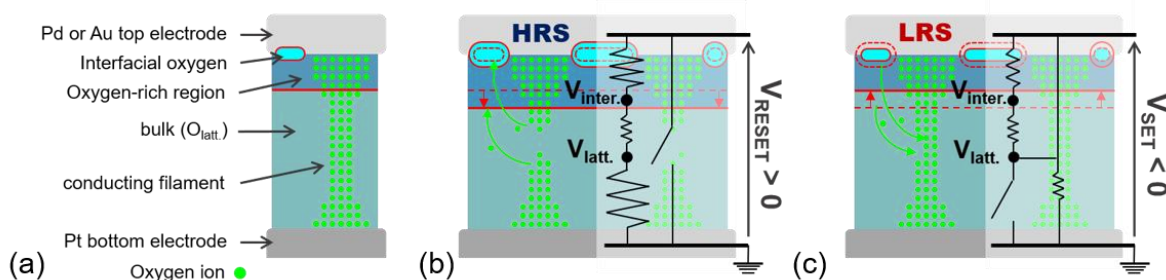
Figure 5 *(a) Sketch of the proposed physical model used to describe the M/LMO/Pt devices (M = Au, Pd) studied by operando HAXPES. Oxygen drift (green arrows) and equivalent circuit of the structure (b) during RESET for $V_{appl.} > 0$ and (c) during SET for $V_{appl.} < 0$. For each stage, the dotted red lines represent the initial state and the continuous lines the final one (i.e. LRS and HRS for SET and RESET, respectively)*

Compiling all these observations, a model of the Pd/LMO interface is depicted in **Figure 5a**. Based on the *operando* analysis of the O 1s and La 3d spectra our system may be divided into three different regions: i) bulk LMO with standard stoichiometry, covered by ii) an oxygen-rich LMO region and, iii) the interfacial oxygen-pocket region. Coming back to the proper stoichiometry of $LaMnO_{3+\delta}$, and considering a homogenous cation concentration, the different regions may be described as:

i) Bulk $LaMnO_{3+\delta}$: $La_{1-x}\square_x Mn_{1-y}\square_y O_{3-\delta}\delta V_O^{\cdot\cdot}$

ii) Oxygen-rich region: $La_{1-x}\square_x Mn_{1-y}\square_y O_3$

being $\square$ the cation vacancies and $V_O^{\cdot\cdot}$ the oxygen vacancies. Excess oxygen occupying interstitial sites is highly unlikely in LMO, as in other perovskites, due to steric effects, which implies the presence of cation vacancies. Having an apparent oxygen-rich region indicates the probable presence of oxygen vacancies in the observed bulk LMO. Thus, the described oxygen drift could be equivalently ascribed to oxygen vacancies motion under the applied electric field.

Based on the electrical characterization results, i.e. ohmic transport in HRS and LRS and abrupt SET and RESET processes, it is most likely that the RS mechanism is related to the formation of conductive filaments. The presence of filaments is also supported by the fact that we only observed small variations of the composition between HRS and LRS, despite a very large change in device resistance.

For the LMO in the filaments to be more conductive than the rest of bulk, these filaments needs to have an oxygen-rich stoichiometry with a larger Mn^{3+}/Mn^{4+} mixed valence state ratio. When a positive voltage (V_{RESET}) is applied, oxygen from the bulk and from the filament drifts toward the top electrode, and consequently oxygen vacancies drift away (see Figure5b). The reduction of the conductive filament drastically reduces its conductivity. Oxygen cannot react with the noble metal electrode and, thus, accumulates at the interface (as deduced from the La 3d spectrum), or is released in gas form between the LMO and top electrode. The resulting state has a slightly more conductive interface but an electrically insulating bulk region, since the filament is broken. The device is therefore in its HRS. When a negative voltage (V_{SET}) is applied oxygen is reintroduced into the material and conductive paths can be formed again: the device is back in its LRS (Figure 5c). Hence, this resistive switching operation can be repeated several times. However, the drawback of this mechanism with inert electrodes is the degradation of the metal/oxide interface due to the accumulation of released oxygen, and the possible formation of gas pockets. Based on these present observations on Pd(Au)/LMO/Pt devices and on our previous results on TiN/LMO/Pt devices[17], it can be concluded that memristive devices using TiN top electrodes are more reliable for non-volatile memory applications due to more reliable redox processes occurring at the TiN/LMO interface, hindering the existence of gas pockets in the latter case.

3. Conclusions

In this work we presented an *operando* HAXPES study of the effect of a chemically inert electrode in a resistive switching device with $LaMnO_{3+\delta}$ as active material. The use of HAXPES in the present contribution has successfully demonstrated its ability to fingerprint modifications of the chemical composition of the LMO/metal interface during resistive switching. The fine analysis of the spectra recorded during the process reveals small changes in the O1s and L3d spectra indicative of the switching mechanism. We demonstrated that in this case the switching

mechanism is different to the one when using a chemically reactive TiN electrode, though it is also triggered by redox reactions and oxygen drift. The main consequence is that oxygen, instead of partially oxidizing the electrode (in the case of the TiN electrode), is here accumulated at the interface, both in a top LMO oxygen-rich layer, and in the form of gas pockets under the metal electrode. This conclusion provides an explanation of the low endurance measured on devices with noble metal electrodes compared to those with TiN, and the severe degradation or lift-off of the electrodes after several RS cycles. These results bring complementary information on the effect of the nature of the top electrode to our previous studies on LMO-based resistive switching devices, providing a good overall view of this system. They show the importance of the choice of the electrode in an oxide-based memory cell device and how it affects both the electrical response and the redox chemistry of the materials that compose the whole system. Although a large HRS/LRS ratio has been demonstrated, desired for ReRAM applications, long time endurance of the device and stability are also critical properties for these devices. Based on our studies, only noble metals would not be suitable to build LMO-based memristive devices; an interlayer acting as an oxygen reservoir (ie. TiN) during operation would be required for optimal operation.

References

[1] I. Gueye, G. Le Rhun, O. Renault, D. Cooper, D. Ceolin, J.-P. Rueff, and N. Barrett, Appl. Phys. Lett. **111**(3), 032906 (2017).

[2] Y. Matveyev, D. Negrov, A. Chernikova, Y. Lebedinskii, R. Kirtaev, S. Zarubin, E. Suvorova, A. Gloskovskii, and A. Zenkevich, ACS Appl. Mater. Interfaces **9**, 43370–43376 (2017).

[3] F. Borgatti, C. Park, A. Herpers, F. Offi, R. Egoavil, Y. Yamashita, A. Yang, M. Kobata, K. Kobayashi, J. Verbeeck, G. Panaccione, and R. Dittmann, Nanoscale **5**, 3954 (2013).

[4] C. Lenser, A. Koehl, I. Slipukhina, H. Du, M. Patt, V. Feyer, C. M. Schneider, M. Lezaic, R. Waser, and R. Dittmann, Adv. Funct. Mater. **25**, 6360–6368 (2015).

[5] P. Calka, E. Martinez, D. Lafond, S. Minoret, S. Tirano, B. Detlefs, J. Roy, J. Zegenhagen, and C. Guedj, J. Appl. Phys. **109**, 124507 (2011).

[6] Y. S. Lin, F. Zeng, S. G. Tang, H. Y. Liu, C. Chen, S. Gao, Y. G. Wang, and F. Pan, J. Appl. Phys. **113**, 064510 (2013).

[7] M. Sowinska, T. Bertaud, D. Walczyk, S. Thiess, P. Calka, L. Alff, C. Walczyk, and T. Schroeder, J. Appl. Phys. **115**, 204509 (2014).

[8] T. Bertaud, M. Sowinska, D. Walczyk, S. Thiess, A. Gloskovskii, C. Walczyk, T. Schroeder, Appl. Phys. Lett. **101**, 143501 (2012).

[9] Y.-L. Jin, Z.-T. Xu, K.-J. Jin, C. Ge, H. B. Lu, and G.-Z. Yang, Mod. Phys. Lett. B **27**(11), 1350074 (2013).

[10] Z.-T. Xu, K.-J. Jin, L. Gu, Y.-L. Jin, C. Ge, C. Wang, H.-Z. Guo, H.-B. Lu, R.-Q. Zhao, and G.-Z. Yang, Small **8**, 1279–1284 (2012).

[11] B. C. Tofield and W. R. Scott, J. Solid State Chem. **10**, 183–194 (1974).

[12] J. Töpfer and J. B. Goodenough, J. Solid State Chem. **130**, 117–128 (1997).

[13] J. A. M. van Roosmalen and E. H. P. Cordfunke, J. Solid State Chem. **110**, 106–108 (1994).

[14] J. A. M. van Roosmalen, P. van Vlaanderen, E. H. P. Cordfunke, W. L. IJdo, and D. J. W. IJdo, J. Solid State Chem. **114**, 516–523 (1995).

[15] S. Bagdzevicius, K. Maas, M. Boudard, and M. Burriel, J. Electroceram. **39**, 157 (2017).

[16] B. Meunier, D. Pla, R. Rodriguez-Lamas, M. Boudard, O. Chaix-Pluchery, E. Martinez, N. Chevalier, C. Jiménez, M. Burriel, and O. Renault, ACS Appl. Electron. Mater. **1**(5), 675–683 (2019).

[17] B. Meunier, E. Martinez, R. Rodriguez-Lamas, D. Pla, M. Burriel, C. Jiménez, O. Renault, J. Appl. Phys. **126**, 225302 (2019).

[18] R. Rodriguez-Lamas, D. Pla, O. Chaix-Pluchery, B. Meunier, F. Wilhelm, A. Rogalev, L. Rapenne, X. Mescot, Q. Rafhay, H. Roussel, M. Boudard, C. Jiménez, and M. Burriel, Beilstein J. Nanotech. **10**, 389–398 (2019).

[19] J. J. Yang, F. Miao, M. D. Pickett, D. A. A. Ohlberg, D. R. Stewart, C. N. Lau, R. S. Williams, Nanotechnol. **20**, 215201 (2009)

[20] L. Tejuca, J. L. G. Fierro, Thermochim. Acta, **147**, 361-375 (1989).

[21] H. Miao, X. Wu, B. Chen, Q. Wang, F. Wang, J. Wang, C. Zhang, H. Zhang, J. Yuan, Q. Zhang, Electrochim. Acta **333**, 135566 (2020).

[22] C. K. Jorgensen, H. Berthou, Chem. Phys. Lett. **13**, 186 (1972).

[23] A. J. Signorelli, R. G. Hayes, Phys. Rev. B **8**(1), 81 (1973).

[24] M. F. Sunding, K. Hadidi, S. Diplas, O. M. Lovvik, T. E. Norby, A. E. Gunnæs, J. Electron Spectrosc. Relat. Phenom. **184**, 399−409 (2011).

[25] J. H. Van Vleck, Phys. Rev. **45**, 405 (1934).

[26] A. T. Kozakov, A. G. Kochur, K. A. Googlev, A. V. Nikolskii, V. I. Torgashev, V. G. Trotsenko, A. A. Bush, J. Alloys Compd. **647**, 947−955 (2015).

[27] E. S. Ilton, J. E. Post, P. J. Heaney, F. T. Ling, S. N. Kerisit, Appl. Surf. Sci. **366**, 475−485 (2016).

[28] V. R. Galakhov, M. Demeter, S. Bartkowski, M. Neumann, N. A. Ovechkina, E. Z. Kurmaev, N. I. Lobachevskaya, Y. M. Mukovskii, J. Mitchell, D. L. Ederer, Phys. Rev. B: Condens. Matter Mater. Phys. **65**, 113102 (2002).

[29] T. Heisig, C. Baeumer, U. N. Gries, M. P. Mueller, C. La Torre, M. Luebben, N. Raab, H. Du, S. Menzel, D.N. Mueller, C.-L. Jia, J. Mayer, R. Wasser,I. Valov, R. A. De Souza, R. Dittmann, Adv. Mater. **30**, 1800957 (2018).

[30] J. L. G. Fierro, L. G. Tejuca, Appl. Surf. Sci. **27**, 453−457 (1987).